Mater. Res. Soc. Symp. Proc. Vol. 874 © 2005 Materials Research Society L5.12.1

A new technique for imaging Mineralized Fibrils on Bovine Trabecular Bone Fracture Surfaces by Atomic Force Microscopy

Johannes H. Kindt, Georg E. Fantner, Philipp J. Thurner, Georg Schitter, Paul K. Hansma

University of California Santa Barbara, Santa Barbara, CA, USA

ABSTRACT

High resolution atomic force microscopy (AFM) images of bovine trabecular bone fracture surfaces reveal individual fibrils coated with extrafibrillar mineral particles. The mineral particles are distinctly different in different regions. In some regions the particles have average dimensions of (70 ± 35) nm along the fibrils and about half that across the fibrils. In other regions they are smaller and rounder, of order (53 ± 14) nm both along and across the fibrils. In other regions they are smaller and rounder, of order (25 ± 15) nm both along and across the fibrils, with more rounded top surfaces.

Significantly, we rarely observed bare collagen fibrils. If the observed particles can be verified to be native extrafibrillar mineral, this could imply that the fractures which created the observed areas propagated within the mineralized extrafibrillar matrix.

INTRODUCTION

The ultra-structure of bone and other mineralized tissues has been studied extensively(1-8). Bone consists of collagen fibrils with diameters on the order of 100nm, a small percentage of non-collagenous proteins, and mineral platelets of carbonated hydroxyapatite (dahllite), also referred to as bone-apatite or bio-apatite (9), with typical dimensions of 27.3nmx11.2 nm for bovine bone with a thickness of 2 - 4nm, as measured by X-Ray scattering (1, 2) and Atomic Force Microscopy (AFM)(10, 11). The mineral platelets can occur both inside and outside collagen fibrils. Fibrils appearing to be covered by mineral have been observed earlier by SEM(12).

Here we present a high-resolution imaging technique of bovine trabecular bone fracture surfaces using AFM.

EXPERIMENTAL DETAIL

Solutions used:

Ca-Buffer: (110mM NaCl, 40mM CaCl2, 10mM Hepes), pH 7.0
Na-Buffer (150mM NaCl, 10mM Hepes), pH 7.0

Bone preparation:

The trabecular parts of bovine vertebrae were stored frozen until they were diced into blocks of 4x4x5mm^3 under constant irrigation using a bone bandsaw (Marmed, Inc. Cleveland, OH, USA), and the marrow was removed with a pressured water system for dental hygiene (Waterpik Technologies, Fort Collins, CO, USA). The outside surface of the trabeculae was then stained with Coomassie Blue R (Sigma-Aldrich, 0.2g/ml) in Na-buffer for 5 minutes, and the samples were rinsed in Ca-buffer to remove excess staining solution. The wet samples were then stored at -20° C in a sealed container until immediately before AFM sample preparation. The maximum handling time at room temperature before fracture and drying was limited to less than 30 minutes in order to minimize sample degradation.

AFM sample preparation:

A stained bone cube was soaked in Ca buffer for 5 minutes, then clamped in a vice, with the natural bone load axis parallel with the vice grip edge, and half of the block extending from the vice. A second vice was then clamped onto the extending half, and pulled away from the first vice to fracture the bone block in tension. The two pieces were then immediately rinsed off briefly in HPLC grade H_2O (EMD, Chemicals, Inc. Gibbstown, NJ), blotted dry on a Kimwipe from the side not exposed by fracture, and separately placed in centrifuge tubes with a small wad of Kimwipe at the bottom. They were then centrifuged for 5 minutes at 1800g to remove any residual buffer and avoid artifacts from salt residues, and dessicated in vacuum for at least 30 minutes. All these steps are designed to prevent any modification of the fracture surface after the fracture event, in particular the formation of salt crystals from the buffer.
To find an area suitable for AFM imaging, we placed the dried cube under a dissection microscope. The Coomassie stain on all surfaces exposed before fracture let us clearly distinguish between stained external surfaces and un-stained fracture surfaces. For AFM, it is important to choose a sample surface that is reasonably smooth. Areas which aren't stained blue, but appear translucent and smooth, not white and rough, turned out to be the most suitable for AFM investigation. Once identified, a trabecula with a promising fracture surface was removed with a scalpel, and embedded in epoxy resin (2-Ton Clear Epoxy, Devcon, Danvers, MA, USA) in a custom-made AFM sample disk with a well in the center, with the surface to be investigated facing upward and exposed roughly parallel to the disk.

AFM setup:

The sample was then set up in an AFM (Multimode, Veeco, Inc., Santa Barbara, CA, USA) equipped with a video microscope (OMV, Veeco) to image sample and cantilever. A Silicon, tapping in air (RTESPW) cantilever was mounted in a multimode glass liquid

cell (13, 14) fitted with an S-shaped silicone O-ring (Veeco). In some cases where the sample disk/epoxy surface was not sufficiently smooth to seal, the O-ring was bonded to the Sample disk using 2-ton epoxy. A dry Nitrogen source was furnished from a dewar filled with liquid nitrogen, a 20 Ohm, 25W power resistor, and a Variac variable transformer (Staco, Energy Products Co., Dayton, OH, USA) (see Figure 1).

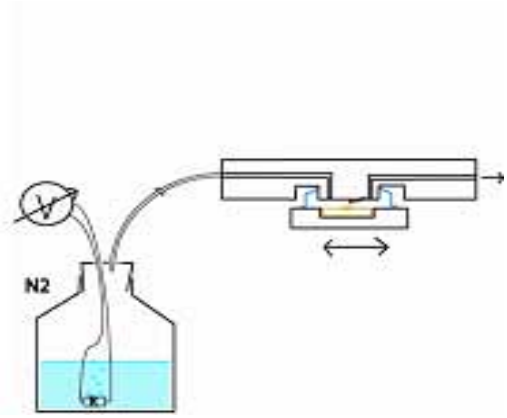

Figure 1: Liquid Nitrogen in a dewar is evaporated at a constant rate by a resistive heater. The N_2 gas reaches room temperature before it enters the AFM fluid cell, which is sealed with a flexible S-shaped Silicone O-ring (Veeco). The N_2 flow rate is controlled by the voltage applied to the resistive heater.

The rate of Nitrogen evaporation inside the dewar is proportional to the amount of heat reaching the dewar inside. The majority of this heat (W) is provided by the resistor inside the dewar, which is connected to the transformer, following $W=V^2/R$. Because the Voltage (U) can be controlled very carefully, and the Resistance (R) is a constant for a given temperature, in this case the boiling temperature of Nitrogen, the nitrogen flow rate of this simple setup is very constant, which is important to guarantee a steady-state temperature and avoid thermal drift inside the microscope which is heated by the laser, and cooled by the flowing gas.
The Dewar was then connected to the liquid cell via several meters of tubing to allow the gas to equilibrate to room temperature before entering the fluid cell. The voltage (V) was set to 7V AC during imaging. The use of dry gas during AFM imaging removes the hydration layer on the sample surface which can affect the sample tip interaction, thereby degrading resolution.

RESULTS

On each sample, the AFM was approached to a smooth fracture surface, and AFM height images with scan sizes of 1um were taken (Figure 2, A-D) in tapping mode under dry N_2 gas, at a scan rate of 1 line/s.
The images show fibrillar structures with diameters on the order of 100-150nm, which appear to be covered with a corrugation which is sometimes knobby and symmetrical (A&B), sometimes plate-like, sharp-edged and elongated along the fibril.
Figure 3, a close-up of Figure 2A, reveals a sharp-edged, crystalline appearance also of these smaller particles.
Particle dimensions where obtained by measuring the maximum edge-to edge distance along and across the fibril axis on 20-40 particles in each of the above images (Figure 4).

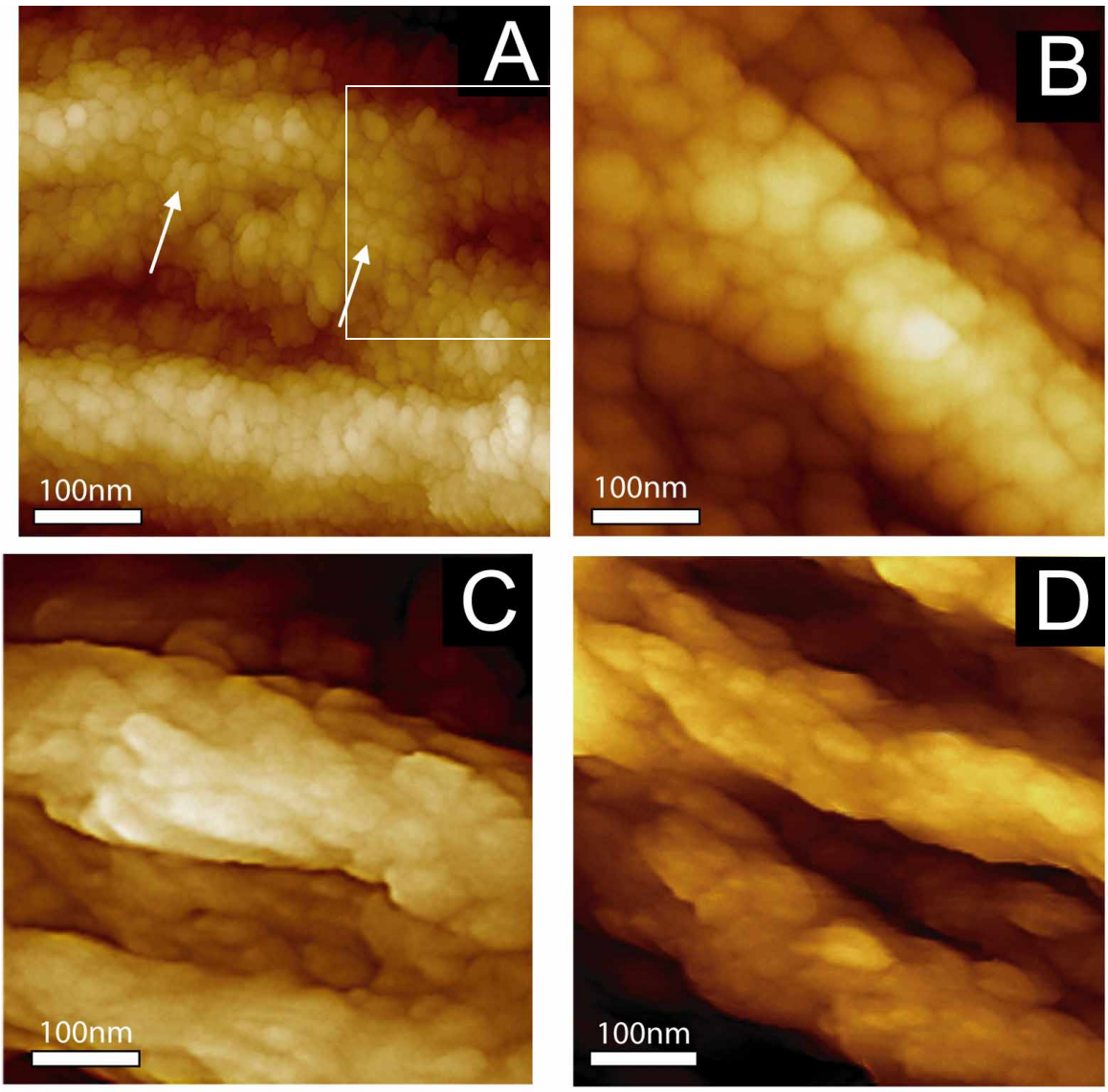

Figure 2:
Mineralized collagen fibrils from four different samples of bovine trabecular bone from vertebrae of the same animal reveal particles of varying shape and size. Particles in (A) and (B) have a round (knobby) appearance. Some particles in (A) appear to fill gaps between fibrils (arrows). Particles in (C) and (D) have more plate-like, crystalline shapes, with the long axis in correlation with the fibril axis, and particles appear to overlap.

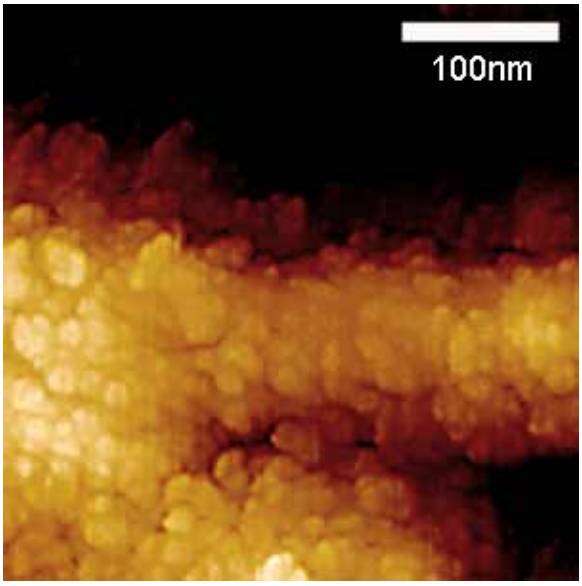

Figure 3: Close-Up From Figure 2A. Scale Bar 100nm.

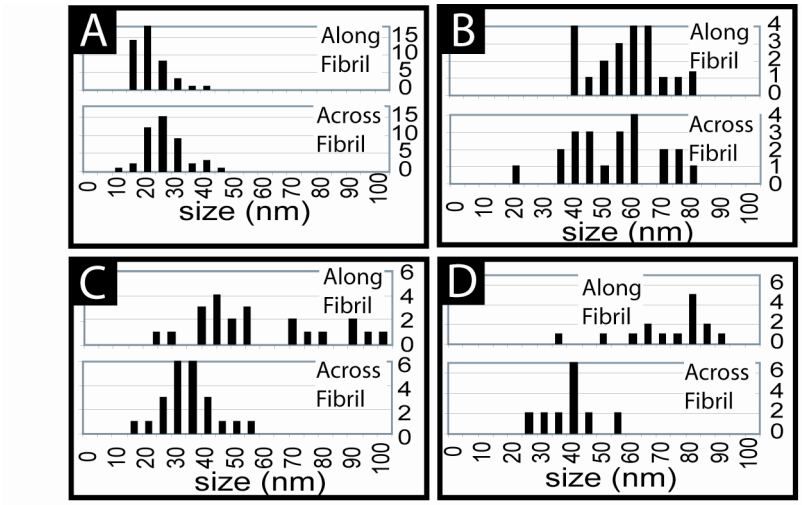

Figure 4:
Histograms of particle dimensions for the corresponding images of Figure 2. The rounded, knobby particles in (A) and (B) show comparable dimensions along and across fibrils of (21±7)nm and (53±14)nm respectively. The plate-like, crystalline particles in (C) and (D) are elongated along the fibril, with large particle length variation in (C): (61±31)nm vs (31±9) nm; and roughly twice the size along the fibril as across the fibril in (D): (74 ±14)nm vs (37 ± 9)nm).

DISCUSSION

The technique presented here portrays fracture surfaces of bovine trabecular bone which were created under near-physiological conditions. While fracturing the bone wet and drying it subsequently brings with it the risk of drying artifacts and deposits on the fracture surface, it also allows to observe a fracture surface which may be closer to the interface responsible for mechanical failure in in-vivo conditions. Care was taken during sample preparation to avoid mineral re-deposition after fracture, however the possibility that the observed particles are artifacts, rather than native extrafibrillar mineral, can not fully be excluded.

The dimensions of the fibrillar structures in Figure 2 are consistent with collagen fibrils. Their particle-like, sharp-edged surface topography is consistent in appearance and dimensions with mineral particles coating the fibrillar structures.

Assuming they are native, the images may show a surface that is the result of a fracture which propagated within the (partially) mineralized extrafibrillar bone matrix.

Further experiments will be necessary to confirm the apatite nature of the observed particles, exclude drying artifacts, and determine whether the fracture propagated within the particle mineral phase or an organic phase surrounding the particles.

The histograms of particle dimensions (Figure 4), while statistically insufficient to reflect the distribution of extrafibrillar mineral in bone, may reveal extrafibrillar particle dimensions which are locally rather consistent, but vary considerably within the same bone over length scales of several um to several mm. The elongated particles in Figure 2 C&D are oriented along the fibril axis. The significance of these differences with regard to bone development or bone mechanical properties is not yet understood.

ACKNOWLEDGEMENTS

We gratefully acknowledge Patricia Turner, Simcha Frieda Udwin and Shreyas Prasad for their invaluable help with researching the literature, Phil Vega for providing bone samples, and Tue Hassenkam for insightful discussions.

This work was supported by the National Science Foundation through the UCSB Materials Research Laboratory under Award DMR00-80034, by the National Institutes of Health under Award GM65354, by the NASA University Research, Engineering and Technology Institute on Bio-inspired Materials (BiMAT at Princeton University under Award NCC-1-02037 (00000532), by Veeco Metrology, by the U.S. Army Research Laboratory and the U.S. Army Research Office under contract number DAAD19-03-D-0004, a doctoral fellowship by ŐAW, the FWF J2395-N02, and SNF PBEZ2--105116.

REFERENCES

1. Fratzl, P., Groschner, M., Vogl, G., Plenk, H., Eschberger, J., Fratzlzelman, N., Koller, K. & Klaushofer, K. (1992) *Journal of Bone and Mineral Research* **7,** 329-334.
2. Fratzl, P., Fratzlzelman, N., Klaushofer, K., Vogl, G. & Koller, K. (1991) *Calcified Tissue International* **48,** 407-413.
3. Petruska, J. A. & Hodge, A. J. (1964) *Proceedings of the National Academy of Sciences of the United States of America* **51,** 871-&.
4. Weiner, S. & Wagner, H. D. (1998) *Annual Review of Materials Science* **28,** 271-298.
5. Landis, W. J., Hodgens, K. J., Song, M. J., Arena, J., Kiyonaga, S., Marko, M., Owen, C. & McEwen, B. F. (1996) *Journal of Structural Biology* **117,** 24-35.
6. Prostak, K. S. & Lees, S. (1996) *Calcified Tissue International* **59,** 474-479.
7. Hassenkam, T., Fantner, G. E., Cutroni, J. A., Weaver, J. C., Morse, D. E. & Hansma, P. K. (2004) *Bone* **35,** 4-10.
8. Habelitz, S., Balooch, M., Marshall, S. J., Balooch, G. & Marshall, G. W. (2002) *Journal of Structural Biology* **138,** 227-236.
9. Pasteris, J. D., Wopenka, B., Freeman, J. J., Rogers, K., Valsami-Jones, E., van der Houwen, J. A. M. & Silva, M. J. (2004) *Biomaterials* **25,** 229-238.
10. Eppell, S. J., Tong, W. D., Katz, J. L., Kuhn, L. & Glimcher, M. J. (2001) *Journal of Orthopaedic Research* **19,** 1027-1034.
11. Tong, W., Glimcher, M. J., Katz, J. L., Kuhn, L. & Eppell, S. J. (2003) *Calcified Tissue International* **72,** 592-598.
12. Braidotti, P., Branca, F. P. & Stagni, L. (1997) *Journal of Biomechanics* **30,** 155-162.
13. Marti, O., Drake, B. & Hansma, P. K. (1987) *Applied Physics Letters* **51,** 484-486.
14. Kindt, J. H., Sitko, J. C., Pietrasanta, L. I., Oroudjev, E., Becker, N., Viani, M. B. & Hansma, H. G. (2002) *Atomic Force Microscopy in Cell Biology* **68,** 213-229.